Electronic Supplementary Information

3 January, 2012

Ms. ID: LC-ART-11-2011-021181

Dual-Electrode Microfluidic Cell for Characterizing Electrocatalysts

Ioana Dumitrescu, David F. Yancey, and Richard M. Crooks

Department of Chemistry and Biochemistry, Center for Electrochemistry, and the Center for Nano- and Molecular Science and Technology, The University of Texas at Austin, 1 University Station, A5300, Austin, Texas 78712-0165, U.S.A.

8 pages

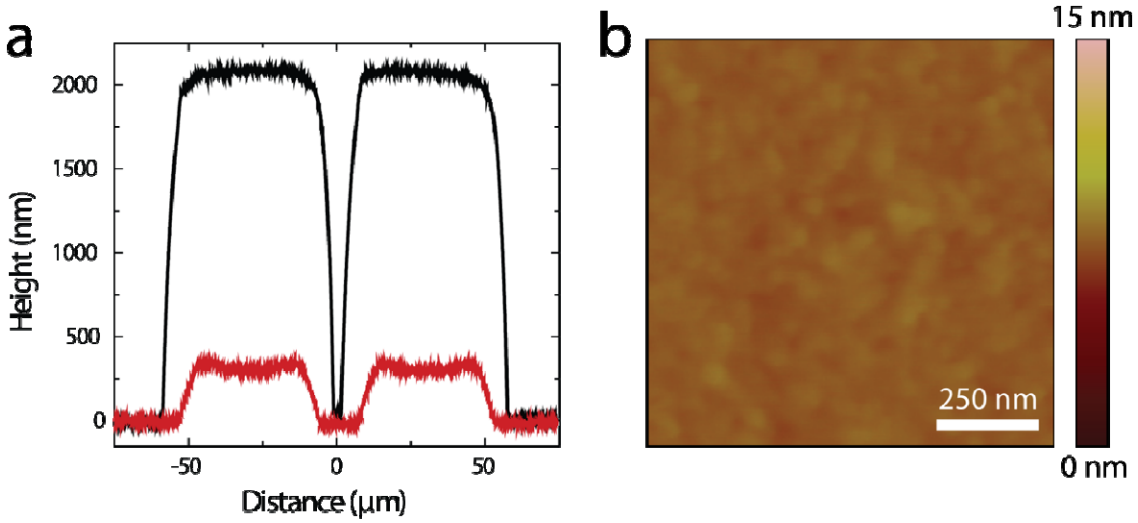

Figure S-1. (a) Profilometry scan lines before (black line) and after (red line) pyrolysis of AZ 1518 photoresist, acquired over the PPC double microband region. After pyrolysis, the width of features decreases from 50 µm to 40 µm, the height decreases from 2000 nm to 300 nm, and there is a slight concavity. The latter effect has previously been observed by others (Lee, J. A.; Lee, S. W.; Lee, K.-C.; Park, S. I.; Lee, S. S. *J. Micromech. Microeng*. 2008, *18*, 035012). Note that the PPC films were found to be strongly adherent to the quartz substrate and could only be removed by scratching with a sharp blade. (b) Tapping mode AFM image of a 1 µm × 1 µm area acquired in the center of a PPC microband. In accordance with previous studies (Ranganathan, S.; McCreery, R. L. *Anal. Chem.* **2001**, *73*, 893), the surface of the PPC microband has an rms roughness of 0.5 nm.

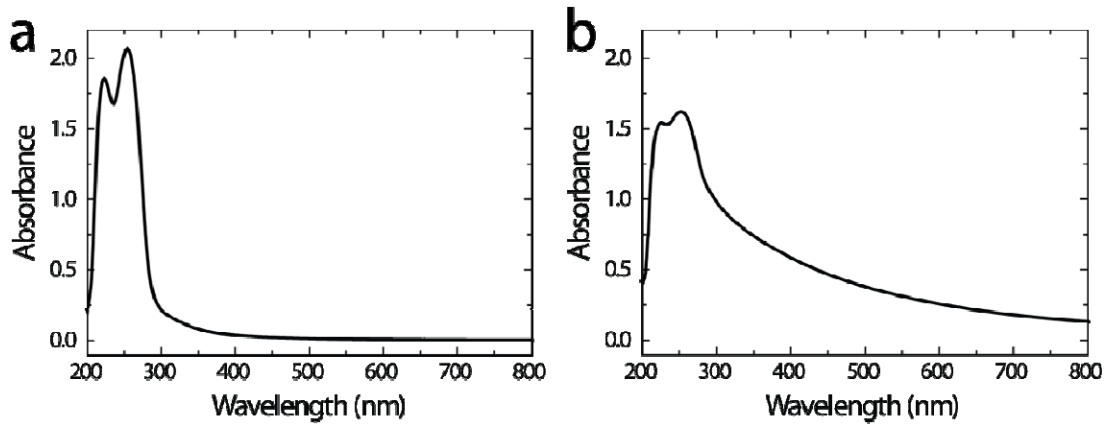

Figure S-2. UV-vis absorption spectra of G6-OH(Pt^{2+})$_{147}$ (a) before and (b) after reduction with $NaBH_4$. The final concentration of G6-OH(Pt_{147}) was 10.0 µM. The DENs spectrum was referenced to a solution containing 10.0 µM of metal-free G6-OH. The optical path length of the cell was 0.20 cm. The spectra are comparable to previous results (Ye, H.; Scott, R. W. J.; Crooks, R. M. *Langmuir* **2004**, *20*, 2915). Absorbances at 220 and 250 nm arise from ligand-to-metal charge-transfer bands associated with Pt^{2+} bound to internal tertiary amines of G6-OH. After reduction, higher absorbances at longer wavelengths are observed, which is characteristic of zerovalent metal particles having nanoscopic dimensions (Kreibig, U.; Vollmer, M. *Optical Properties of Metal Clusters*; Springer: Berlin, **1995**, p. 358)

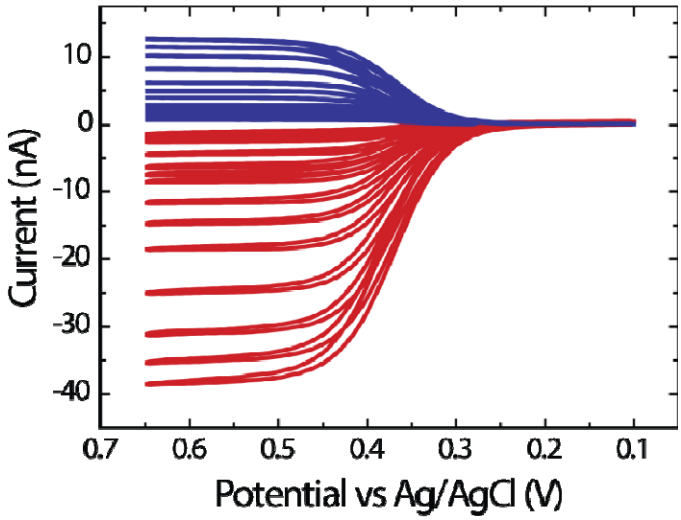

Figure S-3. (a) Full set of generation (red) and collection (blue) CVs from which the partial data set shown in Figure 2a (main text) were extracted. These results were obtained using a solution containing 0.10 mM FcMeOH and 0.10 M KNO_3, and they were acquired over a flow rate range of 0.05 to 100 µL min^{-1}. The PPC microband electrodes were 40 µm long and separated by a 15 µm gap. The microchannel was 6 mm long, 100 µm wide, and 20 µm high. The collector potential was held at 0.0 V (vs Ag/AgCl).

Finite element simulations. For numerical simulations, the microchannel was approximated to a 2D cross-section along the *y* direction (Figure S-4a). In accordance with previous treatments of mass transport to channel flow electrodes (Amatore, C.; Da Mota, N.; Lemmer, C.; Pebay, C.; Sella, C.; Thouin, L. *Anal. Chem.* **2008**, *80*, 9483), edge effects in the *x* direction were assumed negligible.

The velocity profile was determined using the incompressible Navier-Stokes equations for momentum balance (eq 1) and continuity (eq 2) under steady-state conditions (Josserand, J.; Lagger, G.; Jensen, H.; Ferrigno, R.; Girault, H. H. *J. Electroanal. Chem.* 2003, *546* , 1).

$$\rho \mathbf{V} \cdot \nabla \mathbf{V} = -\nabla p + \gamma \nabla^2 \mathbf{V} \qquad (1)$$

$$\nabla \cdot \mathbf{V} = 0 \qquad (2)$$

Here, ρ is the density of water (1.00 g cm^{-3}), $\mathbf{V}$ is the velocity vector (with only component u in the y direction), p is pressure, and γ is the dynamic viscosity of water (1.00 mPa s). For each value of volume flow rate, V_f, employed, the velocity distribution in the microchannel was determined.

The local values of u were used to solve the steady-state convection-diffusion equation (eq 3) for mass-transfer-controlled electrolysis at the two electrodes.

$$\nabla(-D\nabla c) = -\mathbf{V}\nabla c \qquad (3)$$

Here, c the concentration of FcMeOH. The boundary conditions for the Navier-Stokes and the convection-diffusion simulations are summarized in Table S-1.

Table S-1. Boundary conditions used for simulating collection efficiency in the dual-electrode microelectrochemical cell.

boundary	Navier-Stokes boundary	convection-diffusion boundary
1	inlet: velocity $u = V_f / d \cdot h$	inlet: concentration $c_{Fc^+MeOH} = 0$
2	wall: no slip $u = 0$	insulation/symmetry $\mathbf{n} \cdot \mathbf{N} = 0$
3	wall: no slip $u = 0$	insulation/symmetry $\mathbf{n} \cdot \mathbf{N} = 0$
4	wall: no slip $u = 0$	generator: concentration $c_{Fc^+MeOH} = c_b$
5	wall: no slip $u = 0$	insulation/symmetry $\mathbf{n} \cdot \mathbf{N} = 0$
6	wall: no slip $u = 0$	collector: concentration $c_{Fc^+MeOH} = 0$
7	wall: no slip $u = 0$	insulation/symmetry $\mathbf{n} \cdot \mathbf{N} = 0$
8	outlet: no viscous stress $\gamma(\nabla u + (\nabla u)^T)\mathbf{n} = 0$	outlet: convective flux $\mathbf{n} \cdot (-D\nabla c) = 0$

Here, **N** is the inward flux, **n** is the vector normal to a particular boundary, T is the total pressure, and c_b is the bulk concentration of FcMeOH (0.10 mM).

After the concentration profiles at each value of V_f were established (Figure S-4b), the collection efficiency was calculated by dividing the total normal flux, ntflux_c (eq 4), at boundary 6 (collector electrode) to ntflux_c at boundary 4 (generator electrode).

$$\text{ntflux c} = \mathbf{n} \cdot (-D\nabla c + cu) \qquad (4)$$

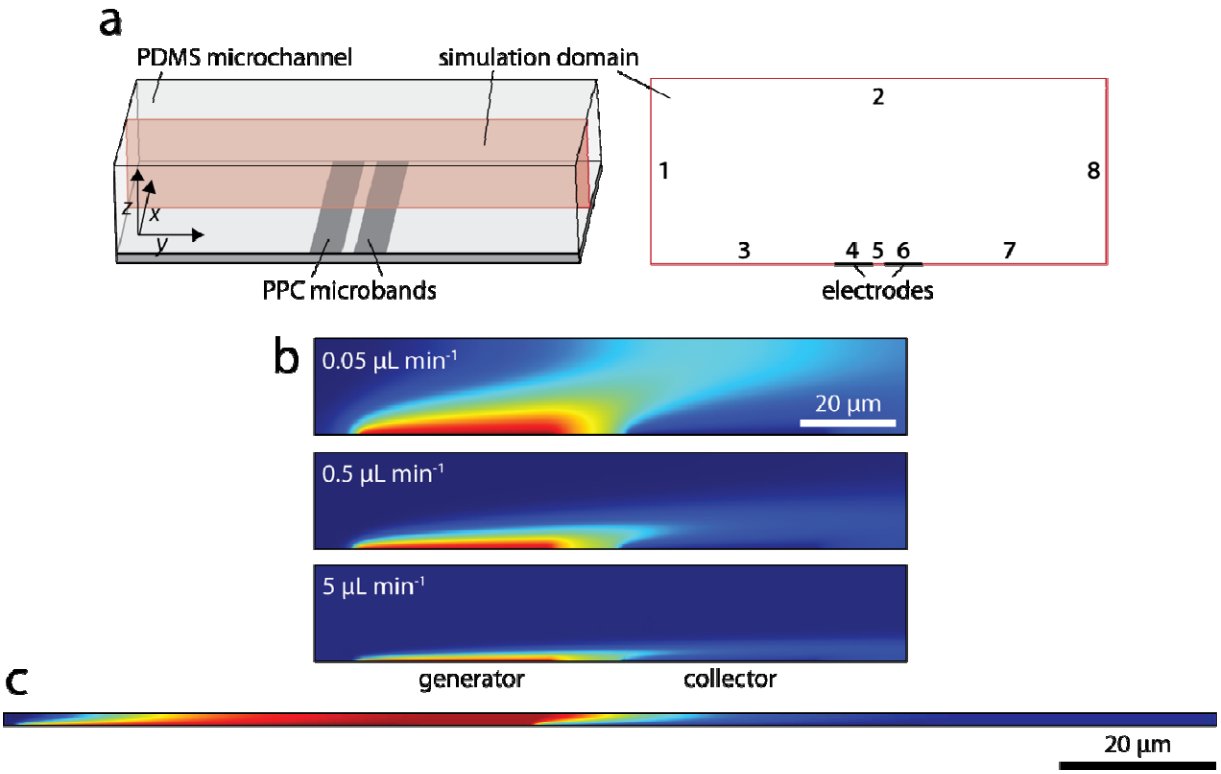

Figure S-4. (a) 2D approximation of the domain used for the finite-element model simulations, showing the numbered boundaries (not to scale). (b) Concentration profiles from generation-collection mass-transfer-controlled electrolysis of a reactant at V_f = 0.05 µL min^{-1}, 0.5 µL min^{-1} and 5 µL min^{-1}. The dimensions are: x_e = 40 µm, h = 20 µm, electrode separation = 15 µm. (c) Concentration profile from generation-collection mass-transfer-controlled electrolysis of a reactant for V_f = 0.01 µL min^{-1}. The dimensions are: x_e = 40 µm, h = 1.5 µm, electrode separation = 15 µm. Calculated collection efficiency is 97.3%. To show the concentration profiles more clearly, in (b) and (c), the simulation domain was cropped.

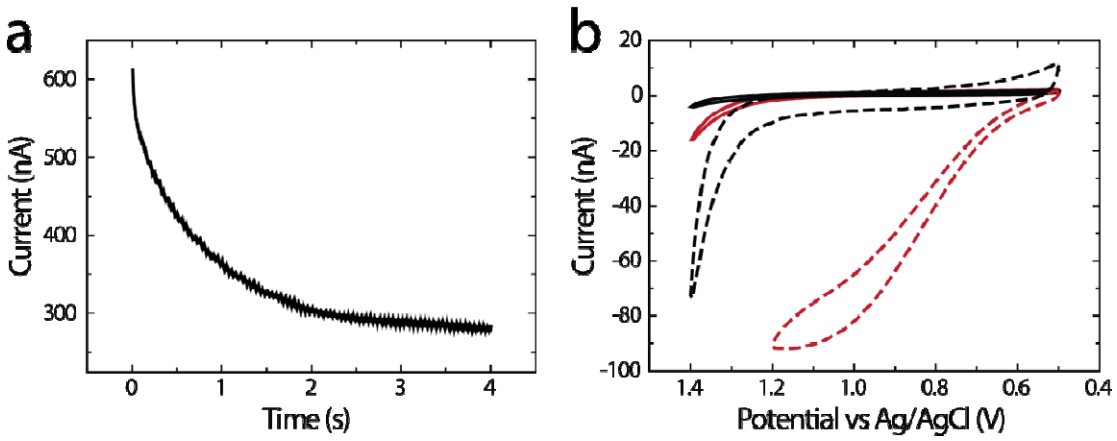

Figure S-5. (a) Platinization current-time curve at the PPC collector electrode, using 1.00 mM K_2PtCl_4 in 0.10 M $HClO_4$, at a flow rate of 0.05 µL min^{-1}. The potential of the electrode was stepped from 0.00 V to -0.40 V (vs Ag/AgCl), well into the reduction wave for Pt^{2+}, for 4 s. (b) CVs recorded at the PPC collector electrode in an aqueous electrolyte solution containing 0.10 M $HClO_4$. The CVs were obtained in absence (black lines) and presence (red lines) of 0.70 mM H_2O_2. The CVs corresponding to the solid and dashed lines were obtained before and after platinization of the collector electrode, respectively. The flow rate was 0.05 µL min^{-1} and the scan rate was 50 mV s^{-1}. At the platinized PPC collector electrode, diffusion-controlled oxidation of H_2O_2 occurs at +1.10 V (vs Ag/AgCl). This potential was chosen for amperometric detection of H_2O_2 at the collector electrode for the ORR measurements described in the main text (Figure 5).